Parallel electron energy-loss spectroscopy and X-ray photoelectron spectroscopy of poly(ether ether ketone)

R. S. Payne*
Cavendish Laboratory, University of Cambridge, Madingley Road, Cambridge CB3 0HE, UK

and G. Beamson
ICI Wilton Materials Research Centre, PO Box 90, Wilton, Middlesbrough, Cleveland TS6 8JE, UK
(Received 28 July 1992)

Electron energy-loss spectroscopy is shown to provide information on the chemical state of carbon atoms in the poly(ether ether ketone) molecule, through comparison with X-ray photoelectron spectroscopy. A careful study of beam damage effects on the energy-loss spectra is presented as a function of electron dose. This ensures that the final results relate to the undamaged polymer, and permits a discussion of the limits of spatial resolution with which the energy-loss technique can be applied to phase-separated systems incorporating an aromatic polymer. The conclusion reached is that energy-loss spectroscopy can provide chemical state information for aromatic polymer systems from regions as small as $140 \times 140\,nm^2$.

(Keywords: poly(ether ether ketone); electron energy-loss spectroscopy; high spatial resolution; X-ray photoelectron spectroscopy; engineering polymer blends)

INTRODUCTION

Poly(ether ether ketone) (PEEK) is a well known thermoplastic, aromatic polymer that was designed by ICI for applications requiring good mechanical performance at elevated temperatures[1,2]. The structure of the PEEK molecule repeat unit is shown in *Figure 1*. Thermoplastics like PEEK have significant advantages over thermoset materials, in terms of their ease of fabrication, repair and reprocessing[3]. The importance of being able to recycle engineering materials has increased the interest in using thermoplastics and in finding techniques that will aid our understanding of the behaviour of blends of thermoplastics.

The transmission electron microscope (TEM) has long been recognized as a tool for investigating blends, and the interfaces in them, because of its potential for imaging and analytical studies at high spatial resolution. However, the polymer scientist often finds that the amount of information available from the TEM is limited by the damaging effect of the electron beam[4,5]. For example, the microanalytical technique of energy-dispersive X-ray (e.d.x.) spectroscopy is difficult to apply to organic systems, because the spectrometer collects a relatively small fraction of the X-rays generated in the sample. This means that high doses are required if good statistics are to be obtained. The information gained in this manner usually bears little relation to the original structure, or for that matter the composition of the sample. Also, e.d.x. spectroscopy offers little in terms of information about the chemical state of the atoms detected. This situation was improved with the advent of commercially available electron energy-loss (e.e.l.) spectrometers. In electron energy-loss spectroscopy (e.e.l.s.) a substantial fraction of the electrons that undergo energy loss are detected, making the technique significantly more efficient for light-element analysis than e.d.x. spectroscopy[6]. A further step forwards in efficiency has been achieved by acquiring the e.e.l. spectrum with a diode array[7] or charged-coupled device (c.c.d.)[8]. When these detectors are used the technique is referred to as 'parallel electron energy-loss spectroscopy' (p.e.e.l.s.), to differentiate it from the old serial acquisition technique, in which the e.e.l. spectrum was scanned across a slit in front of a single photomultiplier tube.

A complete description of e.e.l. processes will not be attempted here; comprehensive reviews of the technique have been written by Egerton[9] and Colliex[10]. However, since the technique is infrequently discussed in polymer literature, it seems appropriate to give a brief description of the spectra that can be obtained. An e.e.l. spectrum consists of two main regions of interest: the low-loss region (0 to 50 eV), and the high-loss region (50 eV upwards). The low-loss region features the zero-loss

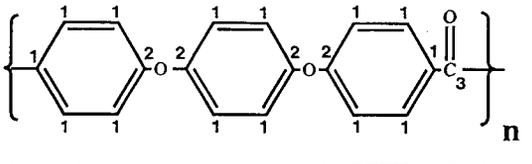

Figure 1 A schematic representation of the PEEK molecule

* To whom correspondence should be addressed

0032-3861/93/081637-07

peak (consisting of unscattered and elastically scattered electrons), and single-electron interband transitions from σ and π bonding orbitals to the unoccupied σ^* and π^* antibonding orbitals. It also contains a broad feature known as the 'bulk plasmon', which is an energy loss arising from a collective oscillation of the 'nearly free' electrons in the system (i.e. the valence electrons)[11]. The high-loss region of the spectrum consists of a monotonically falling background, which is generally approximated by the empirical expression:

$$I = AE^{-r} \quad (1)$$

where A and r are constants, and E is the energy loss. Characteristic ionization edges sit on this background, corresponding to electronic excitations from core levels. Initially the background largely consists of the tail of the bulk plasmon, but each edge contributes to the background on which subsequent edges sit. The number of atoms in the analysed volume that contribute to a particular edge is related to the edge intensity by the equation:

$$I_{\text{edge}}(\alpha,\Delta) = JN\sigma_{\text{edge}}(\alpha,\Delta) \quad (2)$$

Here $I_{\text{edge}}(\alpha,\Delta)$ is the edge intensity, after background subtraction, for a spectrometer collection angle α, and an energy window Δ; J is the number of electrons per unit area that impinge upon the sample; and $\sigma_{\text{edge}}(\alpha,\Delta)$ is the cross-section for the process under consideration. Currently, compositional analysis, based on equation (2), is the most frequently applied aspect of the technique, with well established potential for organic systems.

On the way out of the atom the ejected core-level electrons from each ionization event are involved in transitions to unoccupied molecular orbitals in their spatial vicinity. This results in structure on the ionization edges known as energy-loss near-edge structure (e.l.n.e.s.). It is this structure which can be used as a chemical 'fingerprint', reflecting the chemical state or local environment of the atom type concerned[12,13].

In this paper p.e.e.l.s. is applied to homogeneous thin-film PEEK. Damage effects caused by the electron beam are presented, to demonstrate that spectra can be acquired that relate very closely to the undamaged polymer structure. The low-loss data are used to obtain the real and imaginary parts of the dielectric constant, a fundamental physical property of the material. E.l.n.e.s. at the C_K edge is then studied, and the information contained in this part of the spectrum is compared with that obtained by X-ray photoelectron spectroscopy (x.p.s.) of the PEEK C 1s levels.

EXPERIMENTAL

Specimen preparation

For electron microscopy thin sections of PEEK were cut from PEEK film (ICI Stabar-K200) using an ultramicrotome, and picked up from the surface of deionized water with a conventional 3 mm copper TEM grid (400 mesh). E.e.l.s. was used to estimate the thickness of the sections obtained, from the ratio of the spectral intensity beyond the zero-loss peak to that in the zero-loss peak[9]. An average of the values for 10 regions of sample was 40 ± 5 nm.

X.p.s. samples were prepared by sonicating PEEK film in hexane for approximately 20 min, and mounting on a 10 mm diameter sample stub. An x.p.s. survey scan was performed, showing carbon and oxygen to be the only detectable elements. Quantification of the C 1s and O 1s data gave a surface composition ratio of C:O = 84.4:15.6 at%, in good agreement with the theoretical composition of C:O = 84.2:15.8 at%.

Electron energy-loss spectroscopy

E.e.l.s. was performed in a VG HB501 dedicated scanning transmission electron microscope (STEM) using a field emission source of electrons, operated at 100 keV. A 100 μm objective aperture was used (giving a beam convergence angle of 7.5 mrad). The collection angle of the spectrometer was estimated to be 8.3 mrad. The basic energy resolution of the system was measured from the full width at half-maximum (f.w.h.m.) of the zero-loss peak as 0.6 eV. All of the spectra presented were obtained at a magnification of 500 000 × in area mode, which means that an area of 200×200 nm^2 was scanned by the beam. The spectrometer used features a c.c.d. to detect the electrons, and was built at the Cavendish Laboratory. The spectrometer was operated at a dispersion of 0.15 eV per channel. Prior to the experiment the beam current at the virtual objective aperture of the microscope was compared with that measured by using the spectrometer drift tube as a Faraday cup. This meant that the best possible estimates of the true current at the specimen could be calculated from the virtual objective aperture current at any stage of the experiment.

Experimental conditions similar to those described above can be obtained in conventional TEMs. However, field emission or LaB_6 sources are preferred to tungsten filaments because they provide a narrower distribution of energies: tungsten filaments result in a fundamental resolution limit of around 1.5 eV; LaB_6 sources can provide a limit as low as 0.7 eV.

X-ray photoelectron spectroscopy

X.p.s. spectra were recorded on a Scienta ESCA300 spectrometer, with a rotating-anode monochromized Al Kα X-ray source ($h\nu = 1486.7$ eV). The design and performance of this spectrometer have been described elsewhere[14,15]. Spectra were recorded at 150 eV pass energy and 0.5 mm slit width, giving an instrumental resolution of approximately 0.35 eV. The X-ray source power was 1.4 kW. Charge compensation of the insulating polymer film was achieved using a low-energy electron flood gun (VSW EG2). The optimum charge compensation, as deduced from the spectral resolution, was obtained with the sample at 90° to the electron beam. This orientation corresponds to a photoelectron take-off angle of 45° relative to the sample surface. Spectral acquisition began 15 min after first exposing the sample to the X-ray beam. The C 1s spectrum was completed with sufficient counts in approximately 60 min. X-ray-induced degradation of the sample during such a period is expected to be negligible.

RESULTS AND DISCUSSION

The low-loss e.e.l. spectrum

The low-loss e.e.l. spectrum was studied to demonstrate the ability of e.e.l.s. to provide dielectric information from small volumes of polymer. The real and imaginary parts of the dielectric function can be obtained from low-loss data, and used qualitatively to decide whether features

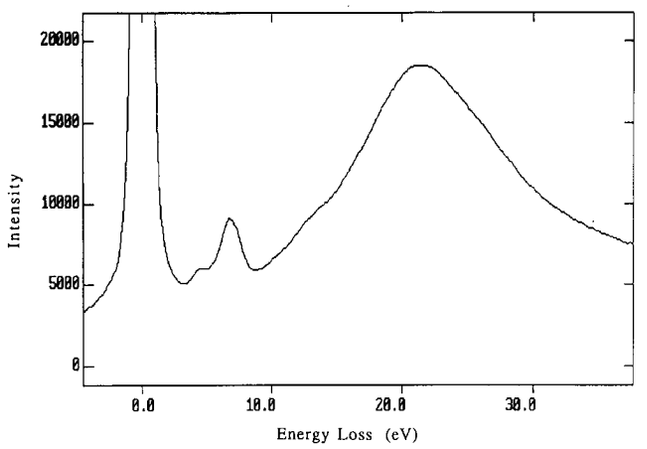

Figure 2 The low-loss region of the e.e.l. spectrum for PEEK

in the spectrum arise from interband, single-electron transitions, or collective oscillations.

Figure 2 is a low-loss spectrum obtained using a beam current of 4.6 pA over a period of 15 s. This corresponds to an electron dose of 10 800 $e^- m^{-2}$, given the magnification of 500 000 ×. The main features in the spectrum are: the zero-loss peak, peaks at 4.4 and 6.8 eV, the large bulk plasmon peak at 21.6 eV and a broad shoulder on the low-energy side of this peak, between 10 and 14 eV. Multiple scattering contributions were removed using the Fourier-log deconvolution method[9], but were in any case small (ranging from zero at the edge onset, to approximately 5% of the signal at 15 eV above onset).

The 4.4 eV peak arises from electronic transitions between π and π^* orbitals of the molecule. The 6.8 eV peak is a feature known as the 'π plasmon'. This feature is well known, and has been documented since the earliest attempts at e.e.l.s. on polymers[16,17]. It arises from the collective oscillation of weakly bound electrons in the π orbitals[18]. The shoulder between 10 and 14 eV is probably due to transitions between σ and σ^* orbitals. These results are similar to those obtained for *p*-terphenylene[19,20], a molecule containing three phenyl groups like those in the PEEK repeat unit, but lacking the ether and ketone linkages. This similarity allows us to reason that the π and upper σ molecular orbitals of PEEK are formed by the delocalized electronic structures of the phenyl groups, with very little contribution from the ring-linking units.

To characterize the electron-beam-induced damage process in the low-loss region of the spectrum, and hence ensure that data like those contained in *Figure 2* were representative, a series of spectra were obtained over a period of 15 s. During this time the sample was exposed to a beam current of 11.7 pA. Each spectrum was acquired in a period of 50 ms, at intervals of 3 s. A similar series was then obtained at a beam current of 21.1 pA. *Figure 3* contains a selection of the spectra obtained at 21.1 pA: the corresponding electron doses per unit area of sample are listed in the figure caption. These data demonstrate that the low-energy peaks in the spectrum decrease in intensity and shift to lower energies as a function of dose. Simultaneously, the background beneath the peaks increases in intensity. The damage process ceases to induce measurable change in the spectrum after a certain dose, leaving a hump between 2 and 7 eV. These changes collectively indicate a disruption of well defined molcular orbitals, and the creation of a wide range of 'defect orbitals'. The final, equilibrium state of the system nevertheless contains a significant fraction of sp^2 or π-bonded atoms. The rise in the background suggests that some of the defect states exist at energies that would normally fall within the band gap for PEEK, i.e. between 0 and about 4 eV.

The π-plasmon intensity above background was calculated and the results plotted as a function of dose, for each of the currents used. *Figure 4* shows these data, along with exponential best fits to the curves. The form of the equation used to fit these data was simply:

$$y = D_0 e^{-\alpha x} + \beta \quad (3)$$

where D_0 is the initial intensity, and α and β are constants. The curves were characterized by finding the dose, $x = 1/\alpha \equiv D_{1/e}$, at which the intensities fell to 1/e of the difference between their original values (D_0) and their final values (β)[21]. For a beam current of 11.7 pA, $D_{1/e}$ was found to be $27\,000 \pm 7000\ e^- nm^{-2}$, whilst for 21.1 pA, $D_{1/e}$ was $17\,000 \pm 5000\ e^- nm^{-2}$. This difference is significant and indicates that the damage process depends not only on the electron dose per unit area but also on the current density. The temperature of a TEM specimen in the region of the electron beam is difficult

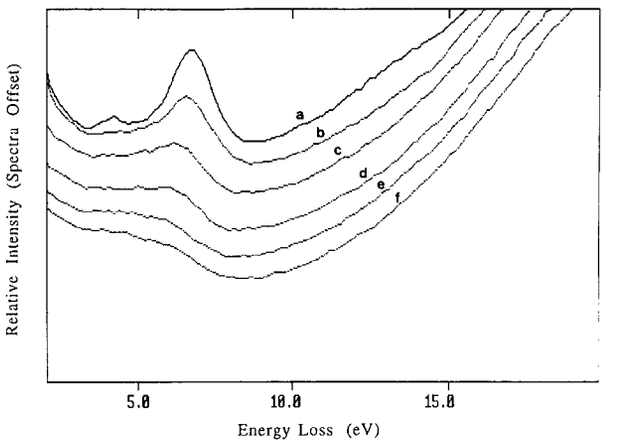

Figure 3 Damage occurring in the π–π^* region of the spectrum, with a beam current of 21.1 pA. Doses ($e^- nm^{-2}$): (a) 0, (b) 10 690, (c) 20 410, (d) 30 130, (e) 39 850, (f) 48 600

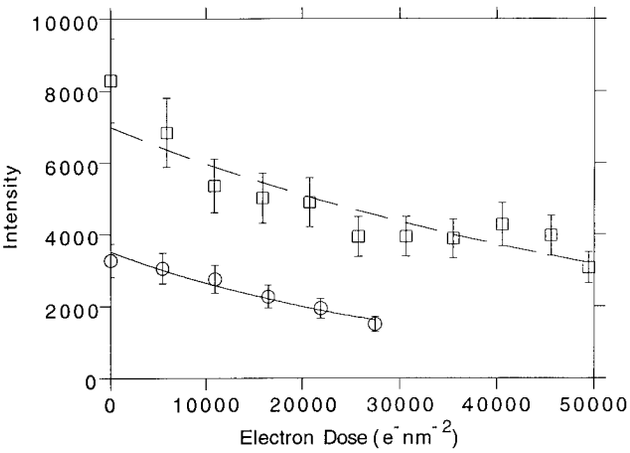

Figure 4 The change in π-plasmon intensity as a function of dose: (○) data for a beam current of 11.7 pA; (□) data for a beam current of 21.1 pA

to estimate. However, it is likely to be higher when the specimen is subjected to a greater current density. Since this is the only obvious difference between the two aforementioned damage rate experiments, we must surmise that thermal effects lead to a reduction in $D_{1/e}$ as the current density is increased. Whilst an increase in specimen temperature will have little or no effect on the cross-section for the e.e.l. processes, it will lead to an increase in segmental movement of the polymer chains. As a result there would be a reduced probability of an sp^2 hybridized bond, broken by an incoming high-energy electron, re-forming. The 'free-radical' chain ends, produced by the bond breaking or scission process, would then have an increased chance of interacting with nearby molecules, to produce sp^3 hybridized crosslinks. Since the intensity of the π plasmon arises largely from the number of sp^2 hybridized bonds in the molecular system, one would expect its intensity to fall more rapidly with dose at elevated temperatures. The corollary of this statement is of course that the re-forming of original bonds might be encouraged by cooling the sample with a liquid-nitrogen or liquid-helium stage[9,21]. Recent work discussing electron-beam-induced damage in organics, and reviewing previous studies of this topic, has been published by Fryer *et al.*[22] and Kurata *et al.*[23].

The beam damage results discussed above show that the spectrum in *Figure 2* was obtained during a period in which the sample received a dose of less than $0.4D_{1/e}$. It should therefore reflect a 'mean state' close to the undamaged state of the molecule.

The zero-loss peak was subtracted from the low-loss data, and Kramers–Kronig analysis was employed to obtain the real and imaginary parts of the dielectric function (ε_1 and ε_2 respectively). The curves resulting from Kramers–Kronig analysis are shown in *Figures 5a* and *b*. The relative shapes of these curves are used to indicate whether peaks in the e.e.l. spectrum are collective (i.e. plasmon-like) or interband in nature. This is possible because the energy-loss function, i.e. spectral intensity, varies in the following way:

$$I \propto \mathrm{Im}(-1/\varepsilon) = \varepsilon_2/(\varepsilon_1^2 + \varepsilon_2^2) \qquad (4)$$

The fact that peaks at 4.04 and 5.44 eV exist in ε_2 whilst ε_1 decreases rapidly through these energies indicates that the features at 4.4 and 6.8 eV have a significant contribution of interband transitions in their nature; ε_2 decreases smoothly, whilst ε_1 increases in the region of the bulk plasmon, confirming the collective electronic nature of this feature[10,18].

The high-loss e.e.l. spectrum: C_K edge

The information held in e.l.n.e.s. is analogous to that provided by X-ray absorption near-edge structure (x.a.n.e.s.). Features in x.a.n.e.s. or e.l.n.e.s. can be used to differentiate between organics that are compositionally equivalent but have different molecular structures. If this capability could be exploited with high spatial resolution, it should find numerous applications in the field of engineering polymer blend research. The C_K edge of PEEK was investigated with this aim in mind.

Figure 6 is an example of a C_K edge from PEEK, after background subtraction and the removal of multiple scattering contributions. These data were obtained by summing 95 spectra, from 15 fresh areas of sample. Each of the 95 spectra was acquired in 2 s, at a beam current of 15 pA, resulting in a maximum dose of 23 440 $e^- nm^{-2}$ for each area. Major features in the spectrum include two relatively sharp leading-edge peaks, separated by 1.54 ± 0.1 eV. In organic systems such peaks are caused by transitions from atomic-like C 1s orbital(s) to π^* molecular orbital(s)[24,25]. Other features in the C_K edge spectrum are: the hint of a further C 1s to π^* peak at 287.5 eV, and peaks corresponding to C 1s to σ^* transitions at 290.2, 293.5 and 301.0 eV. The σ^* states are progressively less well defined in energy, each spreading over several electronvolts.

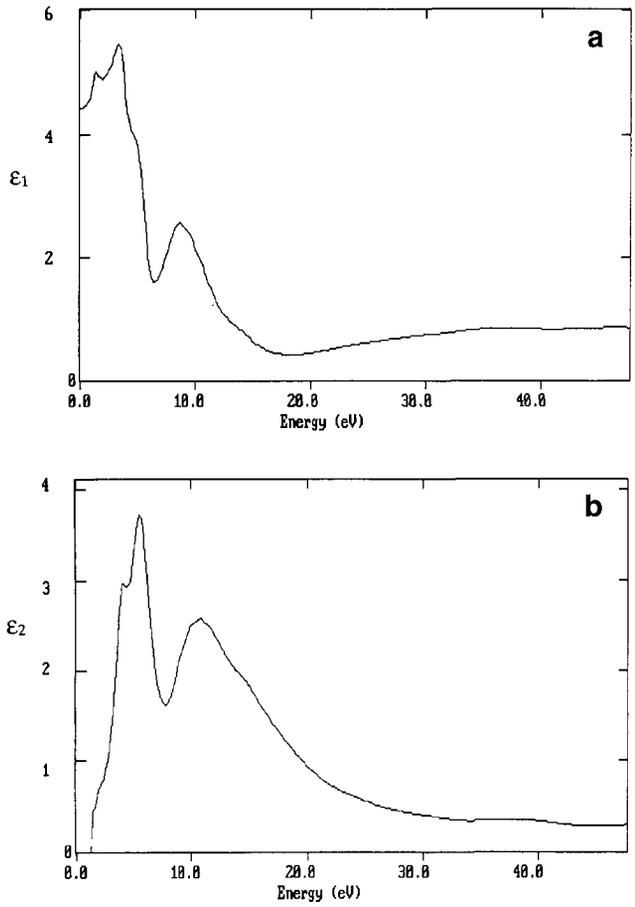

Figure 5 The real part (a) and the imaginary part (b) of the dielectric function

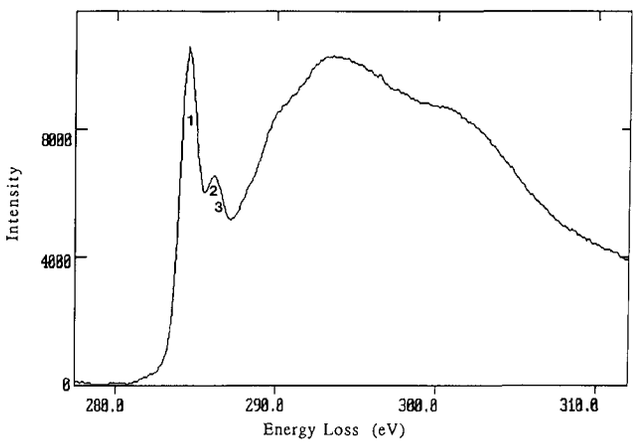

Figure 6 The PEEK C_K edge after background subtraction and correction for multiple scattering. Peaks at the leading edge of the spectrum are labelled according to the x.p.s. interpretation of relevant sites in the PEEK repeat unit (see *Figures 1* and *7*)

It is well known that changes in the binding energy, E_B, of the core levels can occur through different chemical bonding for the excited atom[26]. X.p.s. provides one method of measuring these shifts in E_B. However, if there is only one, well defined π^* molecular orbital for a system, this can act as the final state for transitions from all of the core levels in the molecule. As a result e.e.l.s. can also provide a measure of differences in E_B. To test the validity of this statement, the x.p.s. spectrum of the C 1s levels was obtained for comparison with the e.e.l.s. C_K edge result.

The x.p.s. spectrum of the C 1s levels

The x.p.s. spectrum is contained in *Figure 7*. This figure also displays a fit to the data obtained using the Scienta ESCA300 data-system software. This describes each of the components of a complex envelope as a Gauss–Lorentzian sum function[27], i.e.:

$$F(E)=H\{m\exp[-4\ln(2x^2)]+(1-m)/(1+4x^2)\} \quad (5)$$

$$x=(E-E_0)^2/(\text{f.w.h.m.})^2 \quad (6)$$

where $F(E)$ is the intensity at energy E, H is the peak height, E_0 is the energy of the peak maximum, f.w.h.m. is the full width at half-maximum, and m is the mixing ratio (1 = pure Gaussian, 0 = pure Lorentzian). Asymmetry was introduced with a tail function given by:

$$T(E)=\exp[(-k|E-E_0|)/A] \quad (7)$$

where A is an asymmetry parameter (0 = symmetric, 1 = asymmetric), and k is a constant determined by A and f.w.h.m. The tail was added to the Gauss–Lorentzian sum to give the function Y, defining the peak shape[28]:

$$Y(E)=F(E)+[H-F(E)]T(E) \quad (8)$$

Hence there are five parameters describing each component of the envelope (H, E_0, f.w.h.m., m and A), and two further parameters for the straight-line background. These were input as initial values to the curve-fitting program. On each iteration a 'direction set' method[29] was used to adjust each parameter and minimize the chi-squared value. *Table 1* shows the curve-fit parameters for the PEEK C 1s spectrum contained in *Figure 7*. Components 1, 2 and 3 are due to the three different carbon atoms of the PEEK repeat unit (see *Figure 1*), whilst components 4, 5 and 6 are due to π–π^* 'shake-up' transitions associated with the aromatic ring and the carbonyl group.

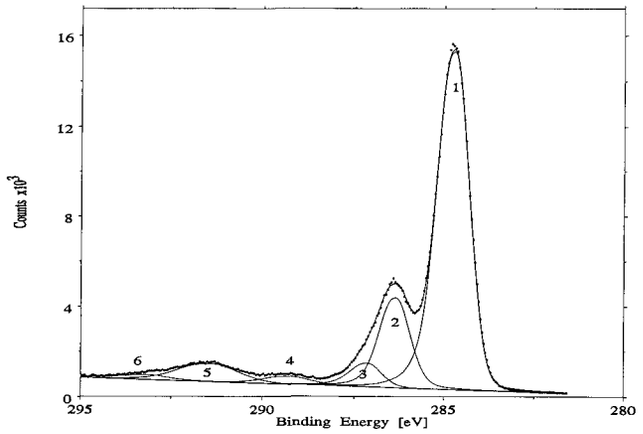

Figure 7 The x.p.s. spectrum of the PEEK C 1s core levels. Peaks at the leading edge of the spectrum are labelled according to the relevant sites in the PEEK repeat unit (see *Figure 1*)

Table 1 Curve-fit parameters for the x.p.s. C 1s spectrum of PEEK

Component	Binding energy (eV)	F.w.h.m. (eV)	Asymmetry parameter	Mixing ratio	Area (%)
1	284.70	1.05	0.12	0.89	66.7
2	286.32	1.02	0.09	0.76	17.8
3	287.10	1.06	0.14	0.78	4.9
4	289.29	1.51	0.06	0.60	2.4
5	291.41	1.94	0.09	0.82	6.6
6	293.09	1.65	0.27	0.15	1.8

The separation of the first two components of the x.p.s. spectrum is 1.38 ± 0.05 eV. This compares well with the separation of the C 1s→π^* components on the leading edge of the e.e.l.s. C_K edge (1.54 ± 0.1 eV). These features apparently arise therefore from transitions from the two C 1s levels to one π^* molecular orbital, or a number of such orbitals that are only slightly different in binding energy. Given the x.p.s. curve-fitting result, it is possible that a third C 1s→π^* component is present in the e.e.l.s. spectrum, separated from the second component by about 0.8 eV. Unfortunately, no sufficiently sophisticated e.e.l.s. fitting routine exists to confirm this at the present time. The e.e.l. process involves two orbitals, the C 1s (which is atomic-like) and the π^* molecular orbital. The x.p.s. process involves transitions from C 1s levels to infinity. This means that the separation of peaks in the e.l.n.e.s. might differ from the corresponding separations in x.p.s., if the binding energy of the π^* orbital is slightly altered at a particular atom site. It would be interesting to plot e.e.l.s. shift against x.p.s. shift, for a range of different carbon atom sites, in a range of different molecules, to gauge the magnitude of such an effect. The conclusion that the PEEK C_K e.l.n.e.s. arise from electronic transitions starting from C 1s levels at three different binding energies could be supported by theoretical estimations of: (i) the shifts in E_B that occur in the molecule, and (ii) the energy of the π^* molecular orbital(s). Such calculations are currently under way in an effort to substantiate this hypothesis about the observed results.

Given that the intensity of both the π-plasmon peak in the low-loss part of the spectrum and the C 1s→π^* intensity in the C_K edge depend on the number of sp^2 hybridized C=C bonds in the system, they are expected to behave in a similar way to electron-beam-induced damage. To investigate this the effects of beam damage on the C 1s→π^* transitions were monitored by again obtaining a series of spectra as a function of dose. In this case the beam current was 15.0 pA. *Figure 8* contains some of the spectra obtained. Each of the spectra shown was acquired in 2 s, at the dose intervals listed in the figure caption. The C 1s→π^* intensity was measured for each of these data sets by subtracting a straight-line fit to the background coming from the C 1s→σ^* transitions. *Figure 9* contains a plot of these intensities as a function of dose, along with a best-fit exponential curve. $D_{1/e}$ was estimated from this curve to be $22\,500\pm6000\ e^-\ nm^{-2}$, which is in good agreement with the figures obtained for the low-loss region of the spectrum. If breaking sp^2 bonds results in the formation of sp^3 bonds, one might expect the C 1s→σ^* intensity in the C_K edge to increase in a manner related to the decrease in the C 1s→π^* intensity. Thus it should be possible to obtain a similar value of

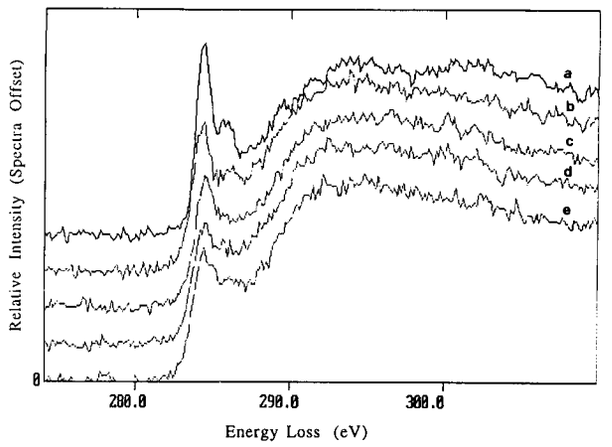

Figure 8 The damage process followed at the C_K edge for a beam current of 15.0 pA. Doses (e^- nm^{-2}): (a) 0, (b) 23 000, (c) 46 000, (d) 69 000, (e) 92 000

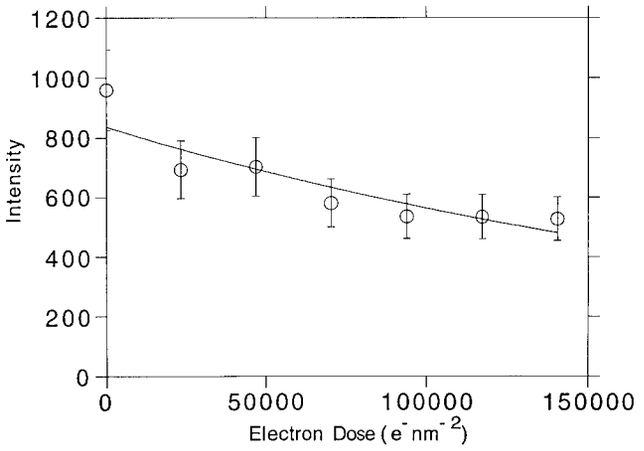

Figure 9 The change in intensity of the C 1s to π^* region of the spectrum as a function of dose: beam current = 15.0 pA

$D_{1/e}$ from each of these spectral features. To test this premise, the intensity of the C 1s→σ^* was measured for the same damage series displayed in *Figure 8*. To ensure that the intensity measured arose from bonds formed during the damage process, it was assumed that the first spectrum in the damage series represented an undamaged PEEK system. These data were scaled to match subsequent spectra in terms of their intensity in the C 1s→π^* region, and then subtracted from each. Intensity was measured by integrating counts over an energy window of 15 eV, between 285 and 230 eV. The results are plotted in *Figure 10*. The decay of intensity in the C 1s→π^* region of the spectrum was adequately modelled by equation (3). If the breaking of sp^2 hybridized bonds leads to the formation of a proportional number of sp^3 bonds, we would expect the C 1s→σ^* intensity to follow the relationship:

$$y' = \gamma D_0(1 - e^{-\alpha x} - \beta) \quad (9)$$

where γ is a constant that takes into account a change in integration window and the probability that more than one sp^3 bond will form for each sp^2 bond broken. Obtaining $D_{1/e}$ for the data in *Figure 10*, using equation (9), gives $25\,000 \pm 6000$ e^- nm^{-2}. This is remarkably close to the value obtained by following the reduction in intensity in the C 1s→π^* region of the spectrum. To the authors' knowledge, this is the first published quantitative evidence demonstrating a strong correlation between electron-induced molecular damage followed in different parts of the e.e.l. spectrum.

Having observed a dose rate dependence, it is illuminating to plot the three values of $D_{1/e}$, obtained for transitions involving the integrity of PEEK π orbitals. This has been done in *Figure 11*. Although the available data are limited, we can tentatively suggest that its continuation to higher dose rates would lead to an intersection with the x axis at 5800 ± 1000 e^- nm^{-2} s^{-1}. *Figure 11* can be used to estimate the practical implications of reducing the area analysed. For example, halving the analysed area would imply a doubling of the typical current density used in this paper to obtain statistically sound data. The current density might go from 2500 to 5000 e^- nm^{-2} s^{-1}. According to *Figure 11*, the resulting $D_{1/e}$ value would be approximately 6000 e^-nm^{-2}. Therefore an acquisition using a dose of $0.5D_{1/e}$ would have to be achieved in approximately 0.6 s. Such an acquisition is just feasible with a manual shift of the sample. These conditions would limit the spatial resolution to an area of 140×140 nm^2. Although such an acquisition would be very difficult to achieve manually, one can conceive of a computer-driven system capable of sampling an area at high magnification, which had been selected at a lower magnification[30]. This is already

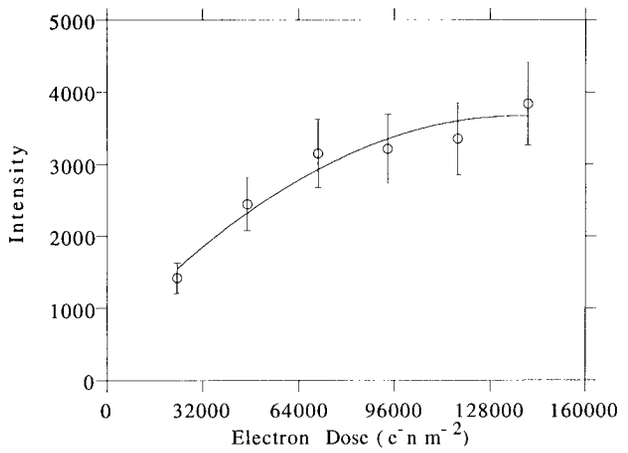

Figure 10 The change in intensity of the C 1s to σ^* region of the spectrum as a function of dose: beam current = 15.0 pA

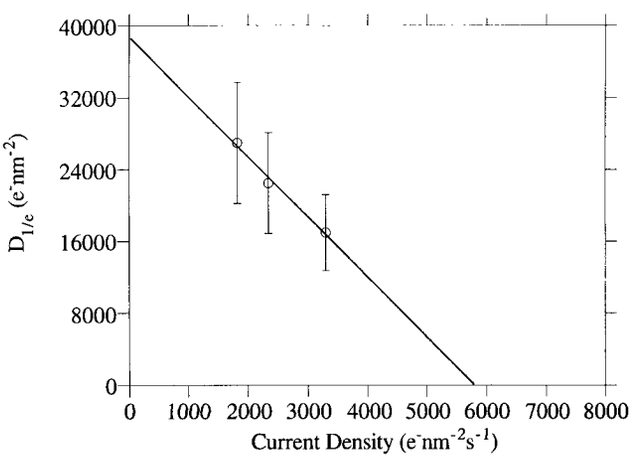

Figure 11 A plot of $D_{1/e}$ against current density

possible on the new generation of conventional TEMs, with their built-in microprocessors[31]. Although there are insufficient data in *Figure 11* to attempt anything other than a straight-line fit, the temperature-dependent steps of the damage process are unlikely to lead to an overall linear dependence of $D_{1/e}$ on dose rate. It seems more likely that the true curve will tend towards a higher value than that predicted by a straight line, giving some hope of a slight improvement in the resolution limit determined by manual manipulation of the sample and changes in magnification.

CONCLUSIONS

The e.e.l. spectrum of polymeric systems contains analogous information to the X-ray photoelectron spectrum of the core levels. E.e.l.s. is capable of providing this information from relatively small regions of material, e.g. an area of $140 \times 140\,nm^2$. It also offers spatially resolved dielectric information for such systems.

The electron beam damage process has been investigated for PEEK, and an estimate has been made of the ultimate dose rate that can practically be applied to this polymer (about $5800\,e^-\,nm^{-2}\,s^{-1}$). This result can be used to predict the smallest area from which information could be obtained. With the limitation of manual specimen shifts, and increases in magnification, useful data could not be obtained from regions smaller than $140 \times 140\,nm^2$. Although this limit was obtained for the PEEK molecule, it is expected to provide a useful benchmark for other aromatic polymers. Greater spatial resolution could be achieved with the aid of a computer-driven low-dose system. The dose rate dependence of the damage process suggests that molecular diffusion plays an important role in the damage process, with elevated temperatures encouraging crosslinking rather than the re-forming of original bonds. As a result, some reduction in the rate of beam damage will be achieved by cooling the sample.

The electron-induced damage process has been successfully followed at the π plasmon, the C $1s \rightarrow \pi^*$ peaks and the C $1s \rightarrow \sigma^*$ region of the e.e.l. spectrum. The expected link between these spectral features has been quantitatively demonstrated.

ACKNOWLEDGEMENTS

The authors would like to thank Professor Peter Rez, Dr David McComb, Dr Athene Donald, Professor Mick Brown and Dr Rik Brydson for their valuable contributions to discussions involving this work. Dr Alastair McGibbon's suggestions on low-dose work in the STEM were extremely valuable, and the technical support of Jon Rickard and Dave Page-Croft was much appreciated. The support of ICI plc's Strategic Research Fund is gratefully acknowledged for the secondment of Dr Robin Payne to the Cavendish Laboratory.

REFERENCES

1 Staniland, P. A. Eur. Pat. Appl. 10868, 1980
2 Wood, A. S. *Mod. Plastics Int.* 1987, 88
3 Christensen, S., Clark, L. P. and Wu, H. *Int. Sampe Symp. Exhib.* 1986, **31**, 1747
4 Misra, M. and Egerton, R. F. *Ultramicroscopy* 1984, **15**, 337
5 Zeitler, E. 'Biophysical Electron Microscopy: Basic Concepts and Modern Techniques' (Eds P. W. Hawkes and U. Valdre), Academic Press, London, 1990, p. 289
6 Ahn, C. C. and Krivanek, O. L. 'EELS Atlas' (ASU HREM Facility and Gatan), Gatan Inc., Pleasantown, CA, 1984
7 Krivanek, O. L., Ahn, C. C. and Keeney, R. B. *Ultramicroscopy* 1987, **22**, 103
8 McMullen, D., Rodenburg, J. M., Murooka, Y. and McGibbon, A. J. *Inst. Phys. Conf. Ser.* 1989, **98**, 55
9 Egerton, R. F. 'Electron Energy-Loss Spectroscopy in the Electron Microscope', Plenum Press, New York, 1986
10 Colliex, C. 'Advances in Optical and Electron Microscopy' (Eds R. Barer and V. E. Cosslett), Academic Press, London, 1984, Vol. 9, p. 65
11 Raether, H. 'Springer Tracts in Modern Physics', Springer-Verlag, Berlin, 1980, Vol. 88, p. 1
12 Brydson, R., Sauer, H., Engel, W., Thomas, J. M. and Zeitler, E. *J. Chem. Soc., Chem. Commun.* 1989, 1010
13 Payne, R. S., Crick, R. A. and McComb, D. W. *Inst. Phys. Conf. Ser. EMAG* 1991, **119**, 113
14 Gelius, H., Wannberg, B., Baltzer, P., Fellner-Feldegg, H., Carlsson, G., Johansson, C.-G., Larsson, J., Munger, P. and Vergerfors, G. *J. Electron Spetrosc. Relat. Phenom.* 1990, **52**, 747
15 Beamson, G., Briggs, D., Davies, S. F., Fletcher, I. W., Clark, D. T., Howard, J., Gelius, U., Wannberg, B. and Baltzer, P. *Surf. Interface Anal.* 1990, **15**, 541
16 Ditchfield, R. W., Grubb, D. T. and Whelan, M. J. *Phil. Mag.* 1973, **27**, 1267
17 Ritsko, J. J. and Bigelow, R. W. *J. Chem. Phys.* 1978, **69**, 4162
18 Fink, J. *Adv. Electron. Electron Phys.* 1989, **75**, 121
19 Hinz, H. J. and Venghaus, H. *J. Chem. Phys.* 1975, **62**, 4937
20 Hermann, A. *Appl. Phys.* 1978, **15**, 185
21 Egerton, R. F. *Ultramicroscopy* 1980, **5**, 521
22 Fryer, J. R., McConnell, C. H., Zemlin, F. and Dorset, D. L. *Ultramicroscopy* 1992, **40**, 163
23 Kurata, H., Isoda, S. and Kobayashi, T. *Ultramicroscopy* 1992, **41**, 33
24 Isaacson, M. *J. Chem. Phys.* 1972, **56**, 1803
25 Isaacson, M. *J. Chem. Phys.* 1972, **56**, 1813
26 Siegbahn, K., Nordling, C., Johansson, G., Hodman, J., Heden, P. F., Hamrin, K., Gelius, U., Bergmark, T., Werme, L. O., Manne, R. and Baer, Y. 'ESCA Applied to Free Molecules' North-Holland, Amsterdam, 1969, p. 104
27 Scienta ESCA300 Users' Manual
28 Sherwood, P. M. A. 'Practical Surface Analysis', 2nd Edn (Eds D. Briggs and M. P. Seah), Vol. 1, 'Auger and X-ray Photoelectron Spectroscopy', Wiley, New York, 1990, p. 574
29 Press, W. H., Flannery, B. P., Teukolsky, S. A. and Vetterling, W. T. 'Numerical Recipes', Cambridge University Press, Cambridge, 1989, p. 294
30 Weiss, J. K., Rez, P. and Higgs, A. A. *Ultramicroscopy* 1992, **41**, 291
31 Philips CM30 Users' Manual